Journal of the Serbian Society for Computational Mechanics / Vol. 6 / No. 1, 2012 / pp. 108-128

(UDC: 616.12-008.318-073)

A mathematical model of arrhythmogenesis in ventricular cardiomyopathies due to gap junction restructuring

A. P. Pirentis[1], **D. Stamenović**[2]*

Department of Biomedical Engineering, Boston University, 44 Cummington St., Boston, MA 02215, USA.
[1]thanospp@bu.edu
[2]dimitrij@bu.edu
**Corresponding author*

Abstract

Genetic defects in cell-cell adhesion sites have been associated with arrhythmogenic ventricular cardiomyopathies (AVCs) and are known to compromise cell-cell coupling. Clinical observations from AVC patients have revealed fibrofatty replacement of healthy heart tissue, which provides an anatomical substrate for arrhythmia, progressive cardiac failure, and sudden death. On the other hand, the absence of fibrofatty tissue in the heart of young patients and in some AVC variants suggests that the observed severe arrhythmias might also occur due to restructuring of gap junctions (GJs) in an environment of degraded mechanical coupling between cardiomyocytes. In this study we develop a mathematical model to investigate the effect of GJ restructuring on arrhythmogenesis in AVCs. We consider a paced ventricular cell-pair and simulate the effect of GJ restructuring by randomly fluctuating the electrical coupling conductance. The emergence of marked arrhythmic episodes is promptly noticed. By further decreasing the fluctuation range with time, propagation fails and action potential generation ceases even before the termination of the stimulus signal. Results from the model simulations are consistent with clinical observations, suggesting an alternative mechanism for the generation of lethal ventricular arrhythmias in AVCs.

Keywords: coupled cells, action potential, gap junction, arrhythmogenic ventricular cardiomyopathy, numerical simulation

1. Introduction

Arrhythmogenic ventricular cardiomyopathies (AVCs) comprise a broad spectrum of lethal heart muscle disorders that are directly associated with genetic defects in desmosomes and fascia adherens junctions at intercalated disk (ICD) cell-cell adhesion complexes (McKoy et al. 2000, Protonotarios and Tsatsopoulou 2004, Tsatsopoulou et al. 2006, Asimaki et al. 2007). The prevalent explanation for this type of diseases suggests that defective cell-cell adhesion is the underlying cause of injury in tissues that bear high, dynamic mechanical loads (McKoy et al. 2000, Tsatsopoulou et al. 2006). A combination of genetic and biomechanical studies in mutation-affected or targeted protein deficiency animal (Ruiz et al. 1996, Yin et al. 2005, Kirchhof et al. 2006) and human (Schnittler et al. 1997, Huang et al. 2008) cell models supports

the above hypothesis. Due to limited regenerative capacity of the myocardium, dying myocytes become replaced by fibrofatty tissue which impedes action potential (AP) propagation and thus provides the anatomical substrate for arrhythmia, progressive cardiac failure, and sudden death. However, clinical studies from certain AVC variants and observations from young human and animal patients (Protonotarios and Tsatsopoulou 2004; Kaplan et al. 2004a,b; Saffitz 2005; Tsatsopoulou et al. 2006), as well as studies of induced protein deficiency in animal ICDs (Kirchhof et al. 2006), have revealed that generation of arrhythmic episodes is possible in absence of marked fibrofatty replacements.

The mechanisms that generate arrhythmic episodes of the latter type are largely unknown. Observations of fewer and smaller conductive channels in AVC cases, however, suggest that a possible explanation is the combination of gap junction (GJ) restructuring in an environment of degraded mechanical coupling and concomitant diminishing of their major constituent protein, Connexin43, at the ICD (Kaplan et al. 2004a,b; Saffitz 2005; Asimaki et al. 2007; Huang et al. 2008). Gap junctions are dynamic channels within ICDs that allow the passage of ions and small molecules between cells (Harris 2001). They are strategically located in close proximity to the other ICD junctions in order to preserve their structural integrity against routine ambient mechanical loads (Kaplan et al. 2004a, Saffitz 2005). Thus, inhibition or mutations in ICD protein components, linked with progressive degradation of cell-cell adhesion, would cause GJs to be exposed to higher than normal mechanical stress. The number and spatial distribution of GJs are principal determinants of electrical current propagation and the temporal/spatial pattern of cardiomyocyte electrical activity (Saffitz 2005). In this study, we model the effect of GJ restructuring on arrhythmogenesis in AVCs.

We use a paced ventricular cell-pair model to simulate the AVC-characteristic restructuring and decrease in number of GJs by fluctuating the coupling conductance of the equivalent circuit. Pacing cell pairs has been successfully used in the past to investigations of AP conduction and electrotonic interactions between cells (Weingart and Maurer 1988; Tan and Joyner 1990; Joyner et al. 1991, 1996; Tan et al. 1991; Morley et al. 1992; Sugiura and Joyner 1992; Wilders et al. 1996; Wang et al. 2000; Huelsing et al. 2001; de Groot et al. 2003). The model simulations demonstrate that, shortly after the onset of fluctuation, impaired electrical coupling results in marked arrhythmic episodes.

2. Model

We consider the equivalent circuit of two identical, electrically coupled ventricular cells (Fig. 1). Each cellular membrane is modeled as a capacitor in parallel with an ionic current due to membrane's ion-channel activity (Keener and Sneyd 2009a). Since GJs aggregate in plaques comprising hundreds up to thousands of channels (Harris 2001), we model the intercellular coupling junction of the equivalent circuit as a tubular conductive channel whose conductivity (G_{GJ}) and cross-sectional area (A_{GJ}) are the sum of the conductivities and cross-sectional areas, respectively, of identical individual tubular GJ channels.

Following the nomenclature of Peercy and Keener (2005), hereafter, subscripts 1 and 2 refer to the cell on the left (*Cell* 1) and the cell on the right (*Cell* 2), and superscripts *i* and *e* refer to the intracellular and extracellular space, respectively (Fig. 1). The total transmembrane current density for *Cell* 1 (I_1^M) is the sum of the densities of the induced capacitive current, the ion channel currents (I_1^{ion}), and an applied stimulus current (I_s), i.e.,

$$I_1^M = C_1^M \frac{dV_1}{dt} + I_1^{ion} - I_s, \tag{1}$$

where $V_1 = V_1^i - V_1^e$ is the transmembrane potential, t is time, and C_1^M is the membrane capacitance per unit area.

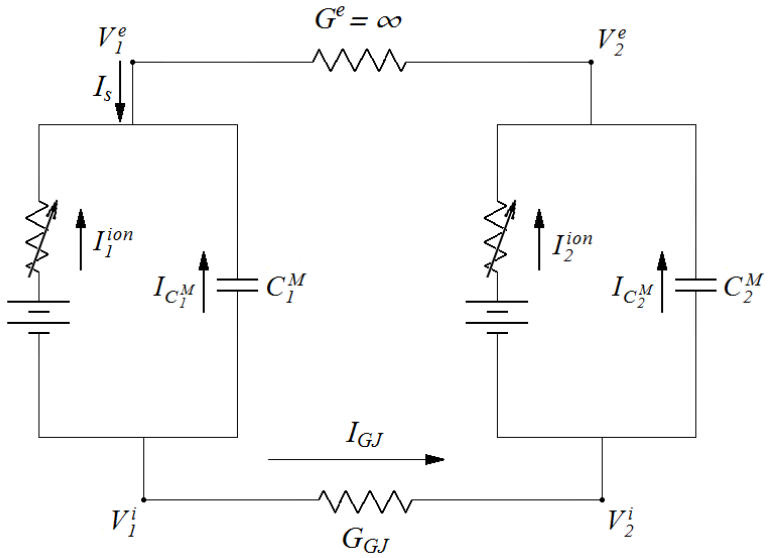

Fig. 1. Schematic representation of the equivalent circuit of two electrically coupled cells. Each sub-circuit comprises a voltage multi-source, variable conductance, and a capacitor, corresponding to the membrane's ionic channels, active and passive resistivity, and capacitance (C1M and C2M). The ionic (I1ion and I2ion) and capacitive ($I_{C_1^M} = C_1^M \left(dV_1 / dt \right)$ and $I_{C_2^M} = C_2^M \left(dV_2 / dt \right)$) current densities are balanced by the current density (IGJ) through the intercellular conductive channel (GGJ); in Cell 1 (left sub-circuit), a stimulus current (Is) is additionally applied (see text for details). The extracellular space is considered to be isopotential (i.e., V1e = V2e)

The current density through the intercellular channel (I_{GJ}) is given by Ohm's law as

$$I_{GJ} = G_{GJ} \left(V_1^i - V_2^i \right). \tag{2}$$

The transmembrane current of *Cell* 1 is balanced by the current through G_{GJ}, i.e., $M_1 I_1^M + A_{GJ} I_{GJ} = 0$, where M_1 is the membrane surface area of *Cell* 1. Assuming that the extracellular space is isopotential, i.e., $V_1^e = V_2^e$, it follows from Eqs. (1) and (2) that

$$M_1 \left(C_1^M \frac{dV_1}{dt} + I_1^{ion} - I_s \right) + A_{GJ} \, G_{GJ} \left(V_1 - V_2 \right) = 0. \tag{3}$$

Following the same reasoning, the current balance for *Cell* 2 is given as

$$M_2 \left(C_2^M \frac{dV_2}{dt} + I_2^{ion} \right) - A_{GJ} \, G_{GJ} \left(V_1 - V_2 \right) = 0. \tag{4}$$

The membrane ionics are modeled according to Beeler and Reuter (1977). The explicit forms of the governing equations are given in Appendix A. Since we assume *Cells* 1 and 2 to be identical, we set $C_1^M = C_2^M \equiv C^M = 1$ μF/cm^2 (Beeler and Reuter 1977), $M_1 = M_2 \equiv M = 5\times10^3$ μm^2 (Peercy and Keener 2005), and $R_1^M = R_2^M \equiv R^M = 1$ kΩ cm^2 (Keener and Sneyd 2009a), where R^M is the passive membrane resistivity. Dividing Eqs. (3) and (4) by the total membrane surface area of the system ($2M$) and multiplying by R^M, we obtain the following coupled ordinary differential equations (ODEs)

$$R^M\left(C_M\frac{dV_1}{dt}+I_1^{ion}-I_s\right)+2\gamma\left(V_1-V_2\right)=0, \tag{5}$$

$$R^M\left(C_M\frac{dV_2}{dt}+I_2^{ion}\right)-2\gamma\left(V_1-V_2\right)=0. \tag{6}$$

Here, I_1^{ion}, I_2^{ion}, and I_s are given in μA/cm^2, V_1, V_2 are given in mV, and time is measured in ms; $\gamma \equiv A_{GJ}\, G_{GJ}\, R^M/2M$ is a non-dimensional parameter that reflects the strength of electrical coupling between the two adjacent cells.

It is straightforward from the definition of γ that (Peercy and Keener 2005):

$$\gamma=\frac{A_{GJ}\,G_{GJ}\,R^M}{2M}=\frac{g_{GJ}\,R^M}{2M}, \tag{7}$$

where $g_{GJ} = A_{GJ}\, G_{GJ}$ is the intercellular channel total conductance. Neglecting the effect of voltage-gate mechanisms and assuming only a single state of conductance (g) for the unit GJ channel, the total intercellular conductance of the equivalent circuit is $g_{GJ} = N{\cdot}g$, where N is the number of unit channels comprising the coupling junction at a given time. Main-state conductances of GJ channels range from a few decades to over 300 pS, depending on the connexin isoform. The unitary conductance of Connexin43 channels is $g \approx 100$ pS (Harris 2001), which for a population of 500 unit channels corresponds to $g_{GJ} = 50$ nS and $\gamma = 0.5$. Consequently, if M and R^M were kept constant, the electrical coupling between the two adjacent cells would be regulated by N and g.

3. Numerical analysis

We simulate physiological and pathophysiological cases by considering different values of model parameters. For the initial junctional conductance (g_{GJ}^0) we use values 0, 5, 15, 35, and 70 nS, which correspond to initial coupling coefficient (γ_0) of 0, 0.05, 0.15, 0.35, and 0.70, respectively, and range from no-coupling at all ($\gamma_0 = 0$), to strong coupling ($\gamma_0 = 0.70$). In all simulations hereafter, we stimulate *Cell* 1 with a train of 1 ms long and 40 μA/cm^2 amplitude pulses (except where stated otherwise), starting at $t = 20$ ms, for each γ_0 value. In order for the simulation to be physiologically relevant, we consider three representative values for the interval between pulses: 750, 500, and 275 ms. If we assume each AP to correspond to a heartbeat, the inter-pulse period of 750 ms results into 80 beats per minute (bpm), roughly the heartbeat rate of an average healthy human adult. The 500 ms period corresponds to120 bpm, a rate that can be characterized as human tachycardia. The 275 ms period is chosen to examine the case where a stimulus is induced inside the refractory period of the preceding AP, based on the typical Beeler-Reuter AP duration of just over 300 ms (Beeler and Reuter 1977).

We first study the constant coupling case, i.e., when $\gamma = \gamma_0$. This case serves as "benchmark" since it is closest to healthy conditions. As the analysis proceeds, the differences between constant coupling and the significantly fluctuating (disease) cases are going to be pointed out. Combining Eqs. (5) and (6) with Eqs. (A.1)-(A.8) from Appendix A, we solve numerically the system of coupled nonlinear ODEs for the following initial conditions: $V_k(0) = -84.62$ mV, $[Ca]_i^k(0) = 10^{-7}$ M, $m_k(0) = 0.011$, $h_k(0) = 0.99$, $j_k(0) = 0.97$, $d_k(0) = 0.003$, $f_k(0) = 1$, $x_k(0) = 0.0074$ (Beeler and Reuter 1977; see Appendix A for definition of these variables). The time-range is from $t = 0$ to 30,000 ms, thus limited only by the need for an adequate enough number of APs for the analysis, and the available computational power.

Action potentials generated in *Cell* 1 by I_s act as stimulus for *Cell* 2. For the 750 ms and 500 ms stimulus periods and $\gamma_0 = 0.05, 0.15$, the electrical activity rhythm between stimulus and *Cell* 1 is 1:1, i.e., each stimulus pulse is associated with one AP in *Cell* 1. For the 275 ms stimulus period, every second pulse fails to produce a new AP resulting in a 2:1 rhythm between stimulus and *Cell* 1. On the other hand, the rhythm between *Cells* 1 and 2 is always 1:1 (Fig. 2a), independent of the stimulus period. When the solution is projected on the $V_2 - x_2$ plane (Jensen et al. 1984), it can be seen from the closed trajectory that the response of *Cell* 2 is periodic (Fig. 2b).

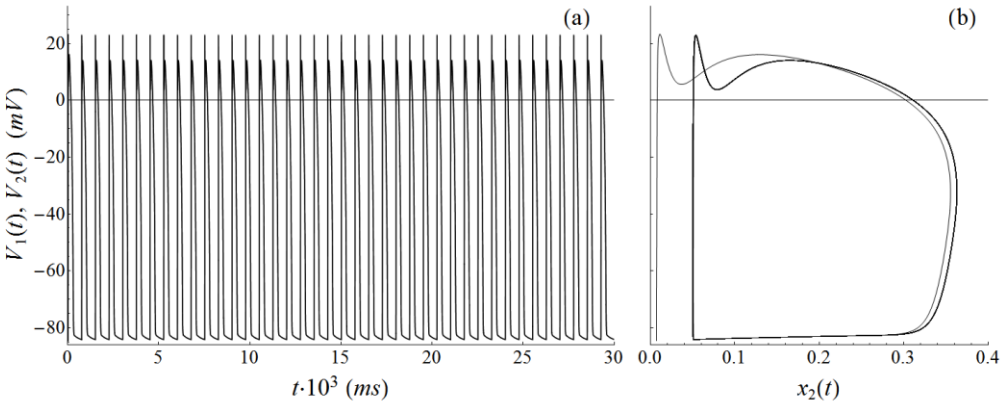

Fig. 2. (a) Full range of the numerical solution for weak constant electrical coupling ($\gamma 0 = 0.05$) and 750 ms stimulus period showing action potentials of Cell 1 (grey trace) and Cell 2 (black trace). Since there is only slight morphological difference between the action potentials of the two cells and their relative electrical activity rhythm is 1:1, Cell 1 membrane potential is over-traced by Cell 2 membrane potential in this resolution. (b) Phase diagram of the solution on the V2 – x2 plane for weak constant electrical coupling ($\gamma 0 = 0.05$) and stimulus period of 750 ms. The closed trajectory of the system implies that the response of Cell 2 to periodic excitation is also periodic

When γ_0 is further increased to 0.35 or 0.70, there is no AP generation either in *Cell* 1, or *Cell* 2. Instead, a train of small duration and amplitude excursions (misfires) from the rest membrane potential is observed in both *Cells*, presenting a 1:1 correlation with the stimulus pulses for all inter-pulse period cases (data not shown). If I_s is slightly increased (e.g., to 45 and 50 μA/cm^2 for $\gamma_0 = 0.35$ and 0.70, respectively), misfires are replaced by full APs, morphologically identical between *Cell* 1 and 2 (data not shown). The observed rhythms are the same as in the weaker coupling cases for the different stimulus periods. Since higher γ_0 corresponds to higher g_{GJ} [see Eq. (7)], the portion of I_s that crosses G_{GJ} from *Cell* 1 to *Cell* 2 (Fig. 1) is greater compared to low γ_0 values. Hence, I_s is not sufficient, unless its amplitude is adequately increased, to excite the membrane of *Cell* 1 to fire a full AP, and hence misfires are observed.

3.1 Random conductance fluctuation

In order to simulate AVC conditions we assume that: i) N fluctuates markedly between an initial population and zero in random fashion, as opposed to healthy conditions where it is assumed to be approximately constant; ii) the cross-sectional area of the N individual channels may decrease relative to the healthy (initial) state, whereas GJ length remains unchanged. Both assumptions imply that $\gamma(t) \leq \gamma(0) \equiv \gamma_0$. We model this behavior by expressing the temporal variation of γ as

$$\gamma(t) = F_{\delta}(t)\,\gamma_0, \tag{8}$$

where $F_\delta(t)$ are interpolation functions (Fig. 3) described in Appendix B. Combining Eqs. (8) and (A1)-(A8), with Eqs. (5) and (6), we solve numerically the system of coupled ODEs for each $F_\delta(t)$ and identical initial conditions as in the constant coupling case. The numerical solution time-range is again 0 to 30,000 ms.

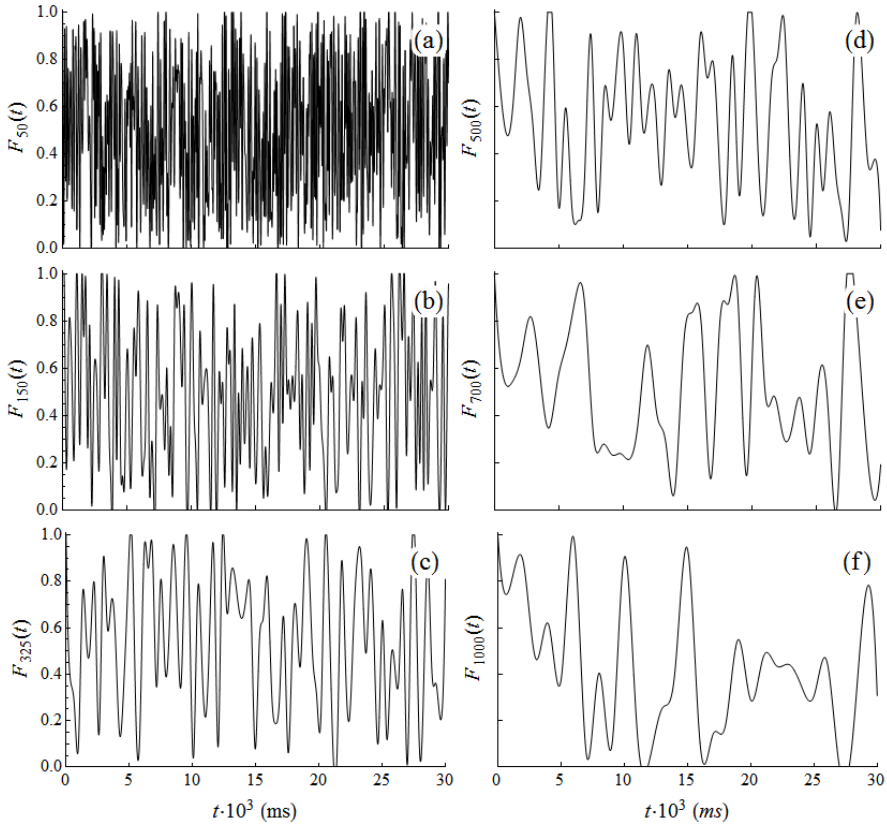

Fig. 3. Fluctuating interpolation functions $F_\delta(t)$ for (a) δ = 50 ms; (b) 150 ms; (c) 325 ms; (d) 500 ms; (e) 700 ms; and (f) 1,000 ms

The response of the system is primarily determined by $F_\delta(t)$ and γ_0. Another parameter that presents a secondary, yet important, effect on the system is the stimulus frequency, as expressed through the inter-pulse period. Thus, depending on the value of $\gamma(t)$ at the time instant when a stimulus pulse is generated, *Cell* 1 responds either with a full AP (γ = 0), a slightly or heavily

distorted AP (very small to small γ values, Fig. 4a,c), or a misfire (intermediate to high γ values, Fig. 4e,g). On the other hand, *Cell* 2 either does not respond at all ($\gamma = 0$), or presents an atypical response (AR) in the form of an amplitude excursion that does not depolarize the membrane (very small γ values, Fig. 4a), or responds with an AP (small to intermediate γ values, Fig. 4c), or a misfire is generated (intermediate to high γ values, Fig. 4e,g).

We first investigate the influence of different values of γ_0 on the coupling for a given $F_\delta(t)$ function and 750 ms stimulus period. For weak initial coupling ($\gamma_0 = 0.05$), $\gamma(t)$ ranges between 0 and 0.05. It is shown above that in the constant coupling case for $\gamma_0 = 0.05$ the rhythm between the two *Cells* is 1:1 (Fig. 2a). On the other hand, it has been established theoretically that if γ is sufficiently low, there is insufficient current flow from a cell that is polarized to a neighboring depolarized cell to raise its potential above threshold (Keener 1990). Therefore, there exists a lower bound γ-value (γ_l) under which APs cannot be generated in *Cell* 2, and for $\gamma = 0$ propagation fails completely. Instead, *Cell* 2 responds with an AR or presents no response at all when $F_\delta(t)$ approaches a zero value (Fig. 4a).

Increasing γ_0 to 0.15 results in $\gamma(t)$ spending less time below γ_l. Consequently, some of the ARs previously observed for $\gamma_0 = 0.05$ are now replaced by APs, whereas the remaining ARs are slightly more pronounced in amplitude (Fig. 4c); no-response at all instances persist for $\gamma = 0$. Further increase of γ_0 to 0.35 and 0.70 results in more ARs being replaced by APs (Fig. 4e,g), with the number of ARs being the smallest for $\gamma_0 = 0.70$. At the same time, due to the relatively high γ_0 values, misfire appearance in both *Cell* 1 and 2 is observed (Fig. 4e,g). In contrast to AR occurrence, misfires can be traced to high values of $F_\delta(t)$, including the unity value. In fact, the number of misfires is always the highest for $\gamma_0 = 0.70$ (Fig. 4g), a trend that is exactly opposite to AR generation. Therefore, there appears to be an upper bound γ-value (γ_u) that renders the generation of APs in *Cell* 1 (and, hence, in *Cell* 2 as well) impossible.

Decreasing the stimulus period to 500 ms yields a response qualitatively similar to the one for the 750 ms case. However, in the 500 ms case the increased stimulus frequency results in generation of more pulses for the same time-range. This, in turn, implies that there are now more responses of each characteristic type for the time intervals where $0 \le \gamma(t) < \gamma_l$, $\gamma_l \le \gamma(t) \le \gamma_u$, or $\gamma(t) > \gamma_u$ in both *Cell* 1 and *Cell* 2.

It is evident that the fluctuation of coupling between zero and a maximum value causes the system behavior to be aperiodic, and this is also verified by the open trajectories of the accompanying phase diagrams in each case (Fig. 4b, d, f, h). Although some of *Cell* 1's APs are now distorted, the electrical activity rhythm between the stimulus and *Cell* 1 is still 1:1 for the 750 ms and 500 ms inter-pulse periods, and for $\gamma_0 \le 0.15$. The appearance of misfires for $\gamma_0 = 0.35$ and 0.70 renders a single rhythm for the entire solution time-range impossible. Similarly, a single rhythm between *Cell* 1 and *Cell* 2 cannot be defined either as *Cell* 2 may respond with an AP, an AR, or no response at all. On the other hand, *Cell* 1 misfires are always associated with misfires in *Cell* 2 as well. Therefore, there is a transition of the system behavior from periodic to aperiodic and vice versa as $\gamma(t)$ scales below γ_l, or above γ_u, and back again. The aperiodic behavior becomes more complicated as the stimulus frequency is further increased. In the 275 ms inter-pulse case, when the first of two successive stimulus pulses results in a distorted AP of *Cell* 1, the reduced duration of the AP implies that the second pulse may also generate an AP since its application corresponds to a time that is now beyond the refractory period of the preceding AP (Fig. 5). Accordingly, more ARs are produced in *Cell* 2. Hence, for the 275 ms case, a unique rhythm cannot be established even between the stimulus and *Cell* 1.

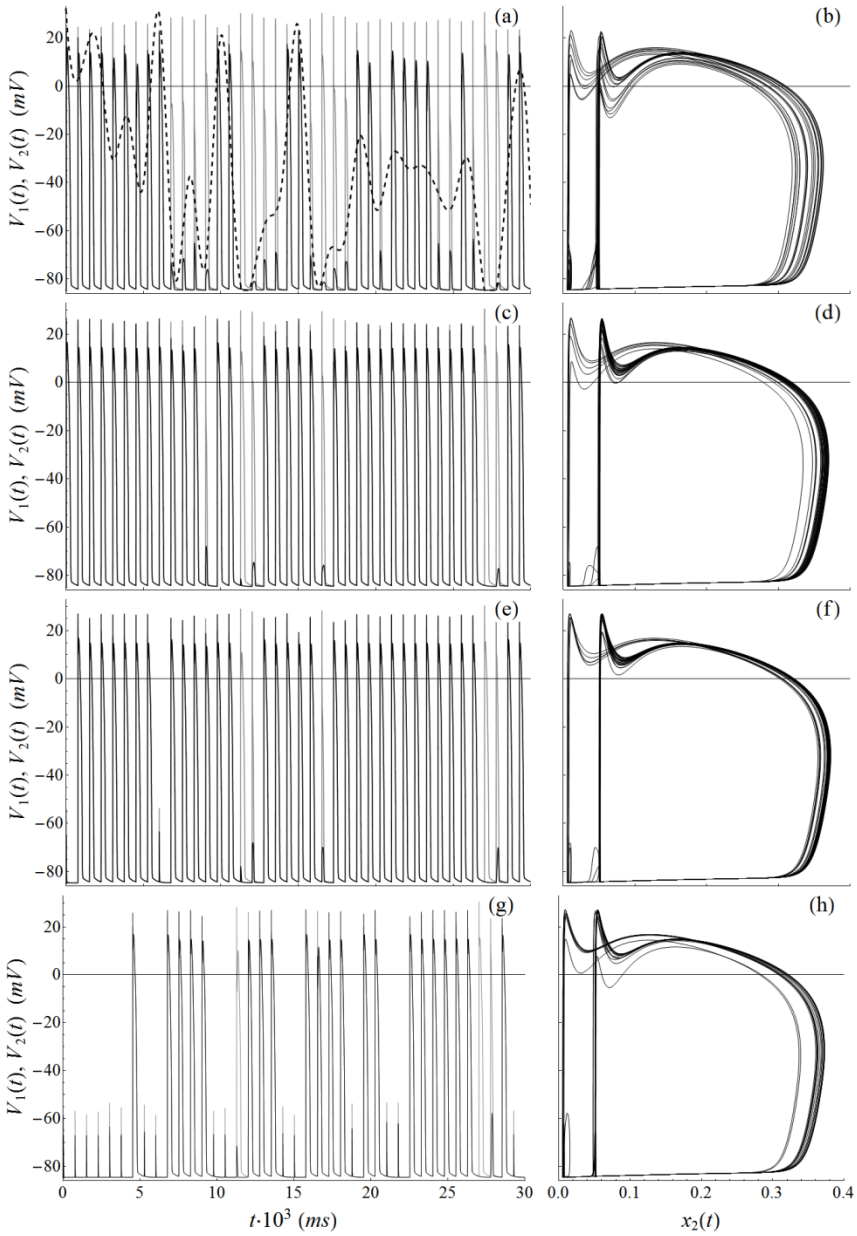

Fig. 4. (a) Full range of the numerical solution for fluctuating coupling, showing action potentials of *Cell* 1 (grey trace) and *Cell* 2 (black trace) for initial electrical coupling of γ_0 = 0.05 and stimulus period of 750 ms; superposition of the interpolation function $F_\delta(t)$ for δ = 1,000 ms (dashed black curve); (b) the corresponding phase diagram of the solution on the $V_2 - x_2$ plane. (c, d) Full range of the numerical solution for fluctuating coupling and corresponding phase diagram on the $V_2 - x_2$ plane for stimulus period of 750 ms, δ = 1,000 ms, and γ_0 = 0.15; (e, f) γ_0 = 0.35; (g, h) γ_0 = 0.70

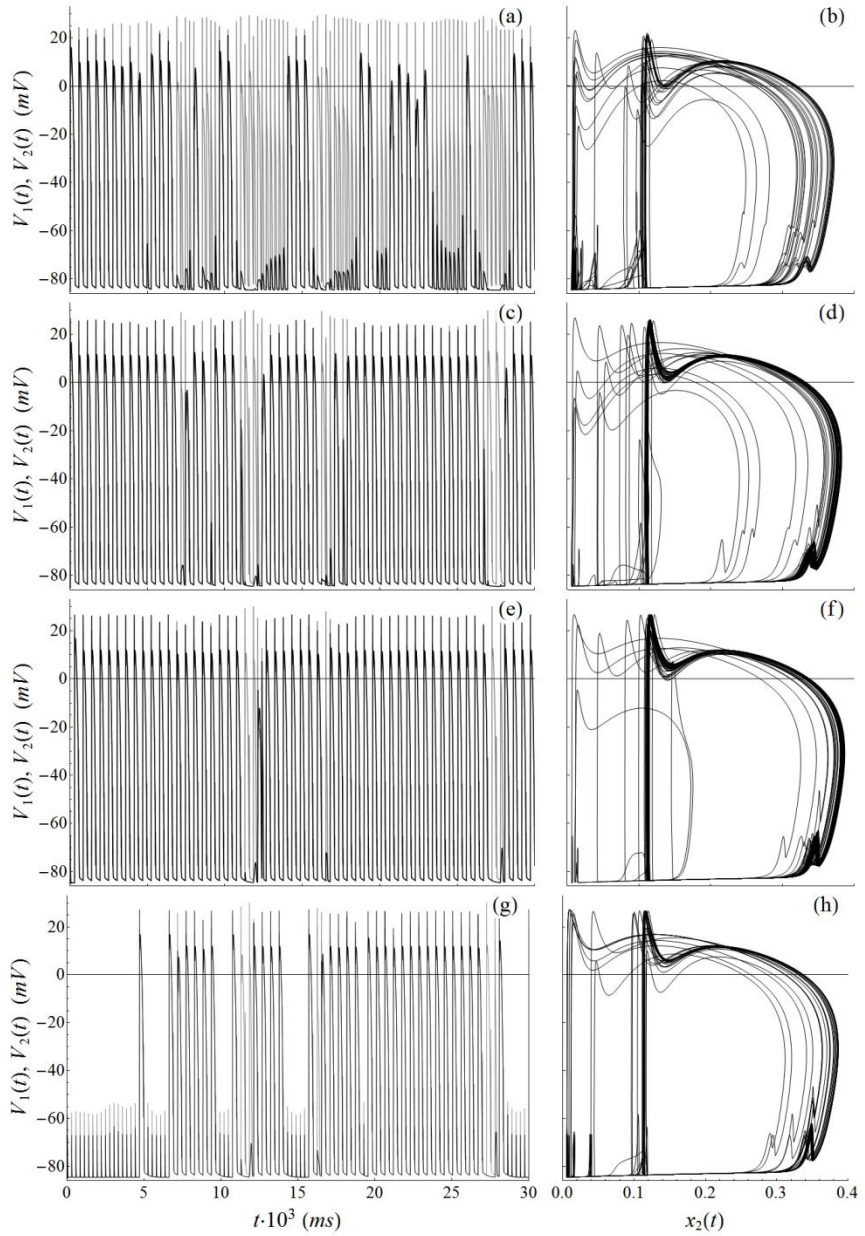

Fig. 5. (a, b) Full range of the numerical solution for fluctuating coupling, showing action potentials of *Cell* 1 (grey trace) and *Cell* 2 (black trace), and corresponding phase diagram on the $V_2 - x_2$ plane for stimulus period of 275 ms, δ = 1,000 ms, and γ_0 = 0.05; (c, d) γ_0 = 0.15; (e, f) γ_0 = 0.35; (g, h) γ_0 = 0.70

Due to the random nature of $F_\delta(t)$, no trend can be identified in the dependence of the number of *Cell* 2's ARs on δ, for a given γ_0 and stimulus period (Fig. 6). In almost all cases, however, there is a greater number of ARs for δ = 1,000 ms than for δ < 1,000 ms (data not shown).

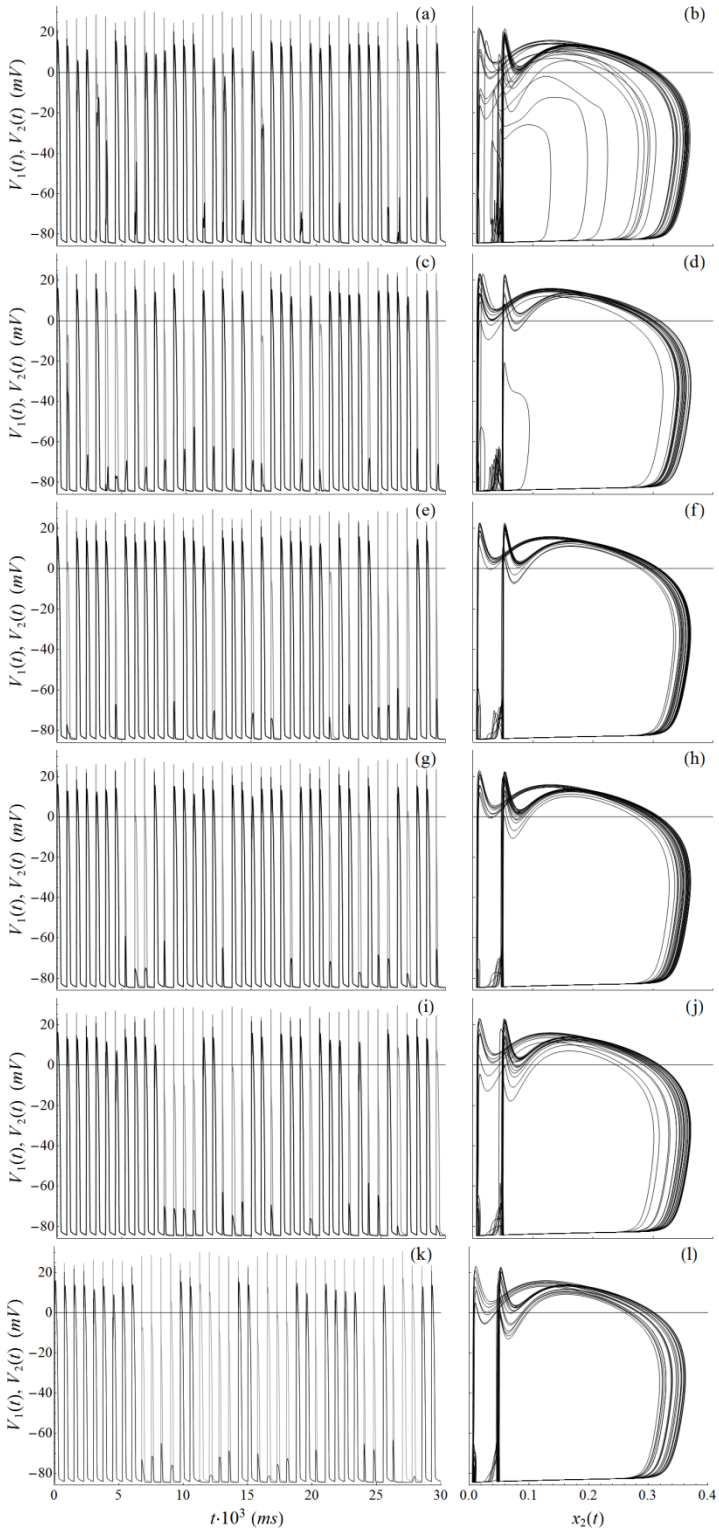
(a)
(b)
(c)
(d)
(e)
(f)
(g)
(h)
(i)
(j)
(k)
(l)
$V_1(t), V_2(t)$ (mV)
20
0
−20
−40
−60
−80
0
5
10
15
20
25
30
$t \cdot 10^3$ (ms)
0.0
0.1
0.2
0.3
0.4
$x_2(t)$

Fig. 6. [PREVIOUS PAGE] (a, b) Full range of the numerical solution for fluctuating coupling, showing action potentials of *Cell* 1 (grey trace) and *Cell* 2 (black trace), and corresponding phase diagram on the $V_2 - x_2$ plane for stimulus period of 750 ms, $\gamma_0 = 0.05$, and $\delta = 50$ ms; (c, d) $\delta = 150$ ms; (e, f) $\delta = 325$ ms; (g, h) $\delta = 500$ ms; (i, j) $\delta = 700$ ms; (k, l) $\delta = 1{,}000$ ms

This is expected since for $\delta = 1{,}000$ ms the variation of $F_\delta(t)$ is the slowest and hence $\gamma(t)$ spends longer time below γ_l than for $\delta < 1{,}000$ ms. The simulations are also inconclusive regarding a possible dependence of the number of misfires on δ, and no δ-value was observed to be systematically associated with the highest number of misfires.

3.2. Decreasing range conductance fluctuation

In order to simulate the long-term effect of AVC disease on AP generation and propagation, we modify the functional expression of $\gamma(t)$ as follows

$$\gamma(t) = H\left(3\times10^4 - t\right) w(t)\, F_\delta(t)\, \gamma_0, \tag{9}$$

where $H(.)$ is the Heaviside step function, $w(t) = 1 - (5/3)\times10^{-5}t - 2[(5/3)\times10^{-5}t]^2$, with $w(0) = 1$ and $w(3\times10^4) = 0$, and t is given in ms. The monotonically decreasing function $w(t)$ (Fig. 7a) acts on $F_\delta(t)$ such that the upper limit of fluctuation progressively decreases and reaches zero at $t = 30{,}000$ ms, for any δ value (Fig. 7). The step function constrains $\gamma(t)$ within the interval $[0, 3\times10^4]$ ms. We solve numerically the system of ODEs, Eqs. (5) and (6), by combining Eqs. (9) and (A1)-(A8) and using the same initial conditions as in the previous two cases. We consider all the values for γ_0, δ, and stimulus period cases as before. The time-range is extended to $t = 35{,}000$ ms in order to observe the system behavior once the two *Cells* are decoupled.

Due to progressive decrease in the upper limit of $\gamma(t)$, at some time $t_{\gamma_l} < 30{,}000$ ms, when γ drops permanently below γ_l, only ARs or no-responses are recorded in *Cell* 2 (Fig. 8) independently of γ_0, δ, or stimulus period. Consequently, AP generation in *Cell* 2 may not be possible long before the actual decoupling between the two *Cells*, and despite the fact that the stimulus signal is active and unaltered. The general behavior of the system for $t < t_{\gamma_l}$ is similar to the case of non-decreasing fluctuating coupling. At $t > 30{,}000$ ms, when the two *Cells* are essentially decoupled, *Cell* 1 response for 750 ms and 500 ms stimulus periods reverts to the respective uncoupled cases (1:1 rhythm), whereas *Cell* 2 membrane potential is kept fixed at rest value for all stimulus periods. In the 275 ms stimulus period case, the response of *Cell* 1 after decoupling is more complex.

Time t_{γ_l} is primarily determined by γ_0, but it is also influenced secondarily by δ and the applied stimulus frequency. For $\delta = 1{,}000$ ms and 750 ms inter-pulse period, t_{γ_l} increases concomitantly with increasing γ_0 (Fig. 8). On the contrary, the numbers of ARs for $t \le t_{\gamma_l}$ and $t_{\gamma_l} < t \le 30{,}000$ ms generally decrease as γ_0 increases. It is straightforward that ARs are more numerous compared to the non-decreasing fluctuation, particularly for the weaker initial coupling cases (Fig. 8a,c). On the other hand, significantly less misfires are observed for the higher γ_0 values, clustered only at the initial stages of the solution (Fig. 8e,g). This observation is in agreement with the eventual permanent drop below γ_u due to progressive decrease in the upper limit of $\gamma(t)$ fluctuation. The exposed dependence of the system behavior on γ_0 for the progressively decreasing fluctuation is reproduced for all δ values and stimulus frequencies (data not shown).

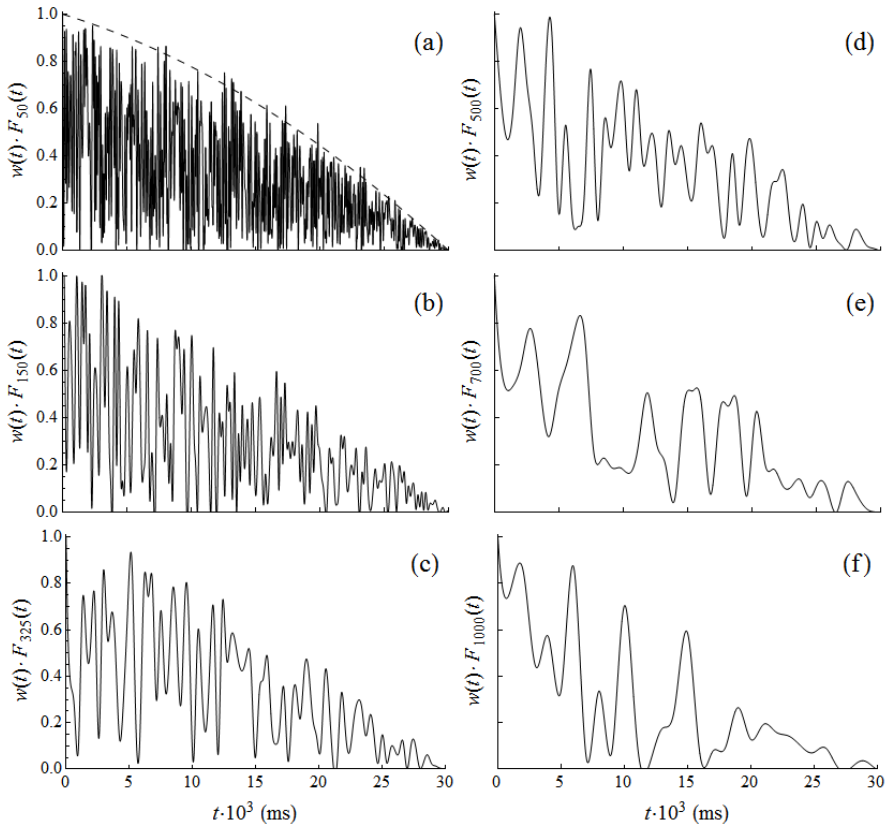

Fig. 7. (a) Effect of $w(t)$ (dashed curve) on the fluctuating interpolation functions $F_\delta(t)$ for δ = 50 ms; (b) 150 ms; (c) 325 ms; (d) 500 ms; (e) 700 ms; and (f) 1,000 ms

The dependence of the system behavior on δ or the stimulus period is less clear. For a given γ_0, no unique correlation can be sketched between t_{γ_l} and δ (Fig. 9). The only notable observations are that the variation of t_{γ_l} with δ for a given γ_0 decreases at higher values of γ_0, and that the t_{γ_l} associated with δ = 1,000 ms is always the smallest (data not shown). The latter can be justified by considering, again, the fact that the slowest variation of $F_\delta(t)$ makes it less likely for the coupling to rebound once having dropped below γ_l, compared to the lower δ values. Moreover, a change in stimulus frequency seems to influence the small-valued γ_0 and δ cases, but leaves the strong initial coupling and slow fluctuation relatively unaffected (data not shown).

For the 750 ms and 500 ms inter-pulse cases, the electrical activity rhythms between stimulus and *Cell* 1 are 1:1 throughout the solution range (Fig. 8), whereas for a 275 ms inter-pulse period the rhythm cannot be uniquely defined before decoupling. After decoupling, and until the end of the numerical solution period, the rhythm between stimulus and *Cell* 1 may, or may not, revert to 2:1 (Fig. 10), i.e., to the rhythm of the corresponding uncoupled case. Whether or not the transition occurs depends on the response of *Cell* 1 to the very last two stimuli prior to decoupling time (t = 30,000 ms), which, in turn, depends on γ_0 and $F_\delta(t)$.

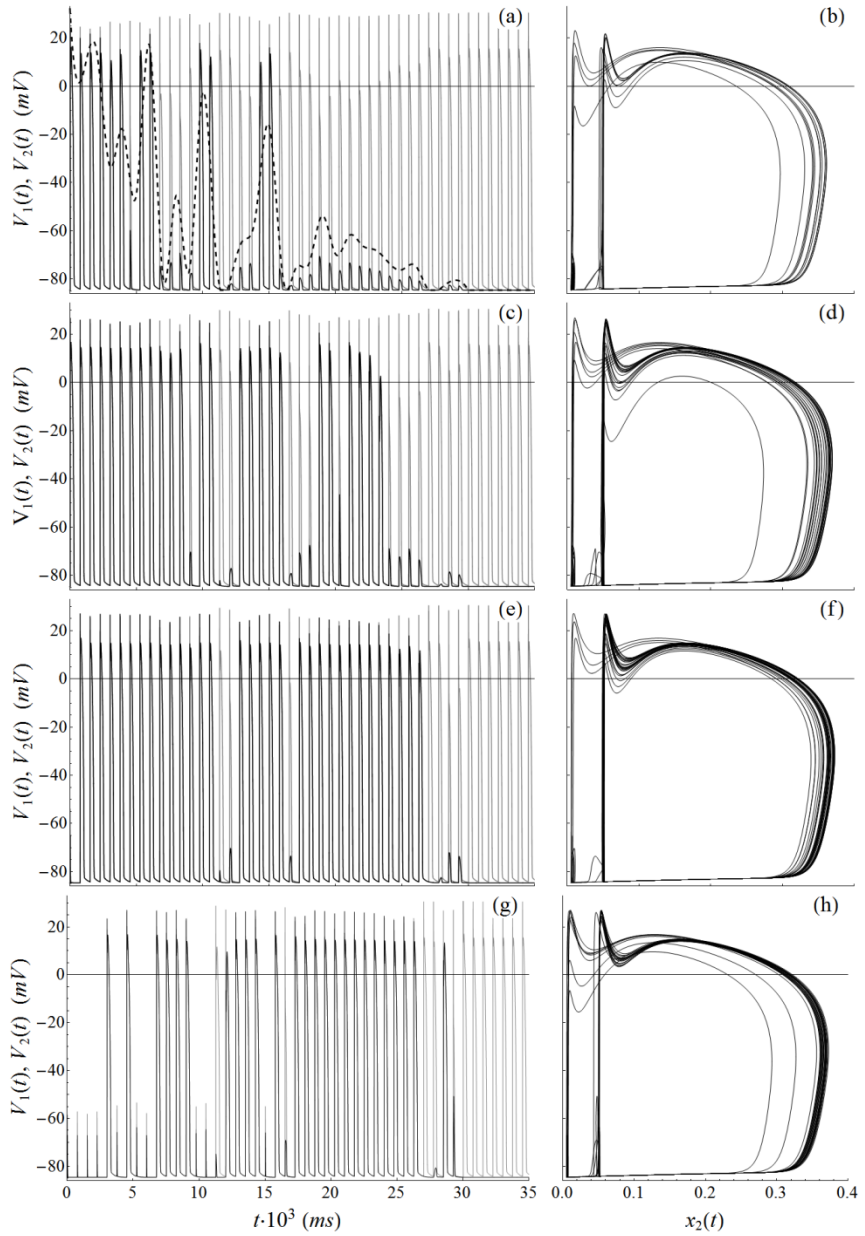

Fig. 8. (a) Full range of the numerical solution for progressively decreasing fluctuating coupling, showing action potentials of *Cell* 1 (grey trace) and *Cell* 2 (black trace) for initial electrical coupling of $\gamma_0 = 0.05$ and stimulus period of 750 ms; superposition of the function $\gamma(t)/\gamma_0$ as given by Eq. (9) for $\delta = 1{,}000$ ms (dashed black curve); (b) the corresponding phase diagram of the solution on the $V_2 - x_2$ plane. (c, d) Full range of the numerical solution for progressively decreasing fluctuating coupling and corresponding phase diagram on the $V_2 - x_2$ plane for stimulus period of 750 ms, $\delta = 1{,}000$ ms, and $\gamma_0 = 0.15$; (e, f) $\gamma_0 = 0.35$; (g, h) $\gamma_0 = 0.70$

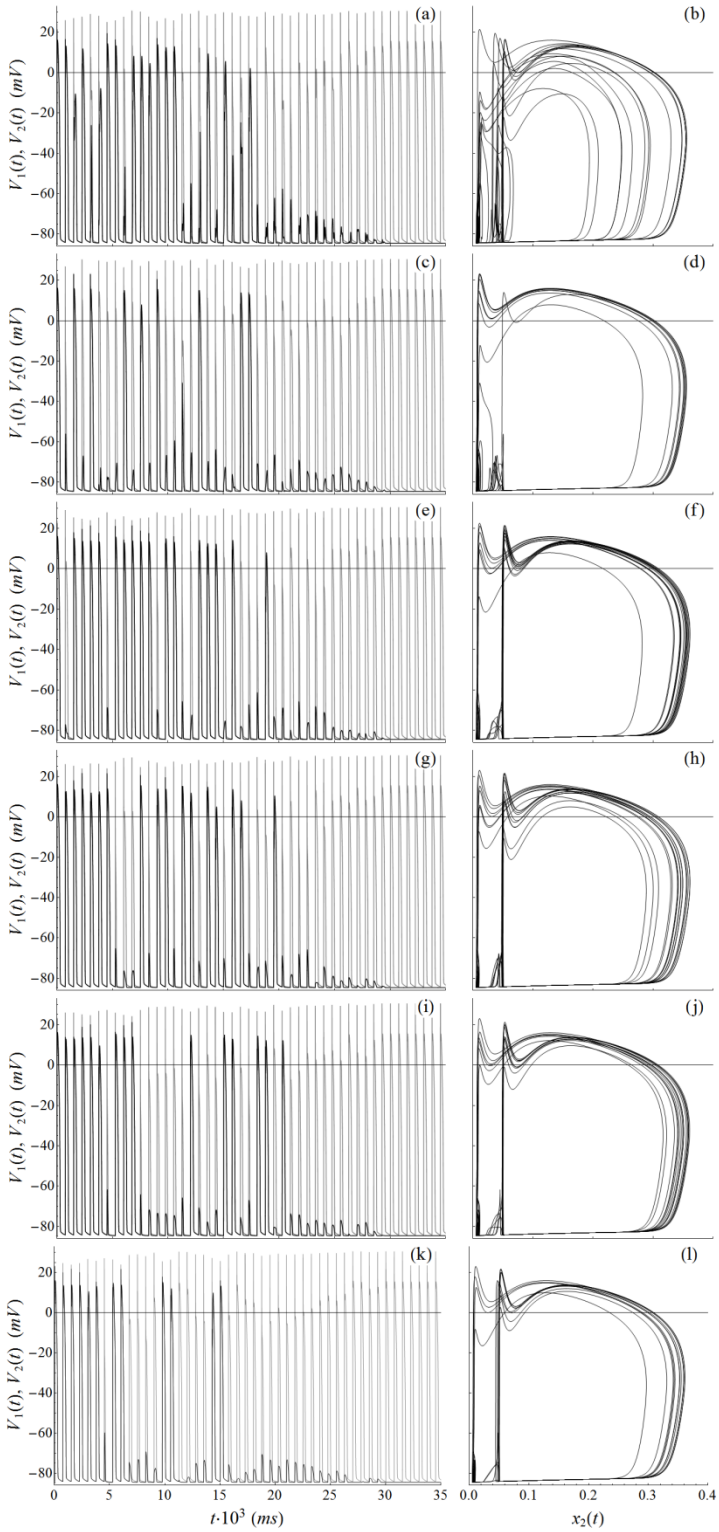
(a)
(b)
(c)
(d)
(e)
(f)
(g)
(h)
(i)
(j)
(k)
(l)
$V_1(t), V_2(t)$ (mV)
20
0
−20
−40
−60
−80
0
5
10
15
20
25
30
35
$t \cdot 10^3$ (ms)
0.0
0.1
0.2
0.3
0.4
$x_2(t)$

Fig. 9. [PREVIOUS PAGE] (a, b) Full range of the numerical solution for progressively decreasing fluctuating coupling, showing action potentials of *Cell* 1 (grey trace) and *Cell* 2 (black trace), and corresponding phase diagram on the $V_2 - x_2$ plane for stimulus period of 750 ms, $\gamma_0 = 0.05$, and $\delta = 50$ ms; (c, d) $\delta = 150$ ms; (e, f) $\delta = 325$ ms; (g, h) $\delta = 500$ ms; (i, j) $\delta = 700$ ms; (k, l) $\delta = 1{,}000$ ms

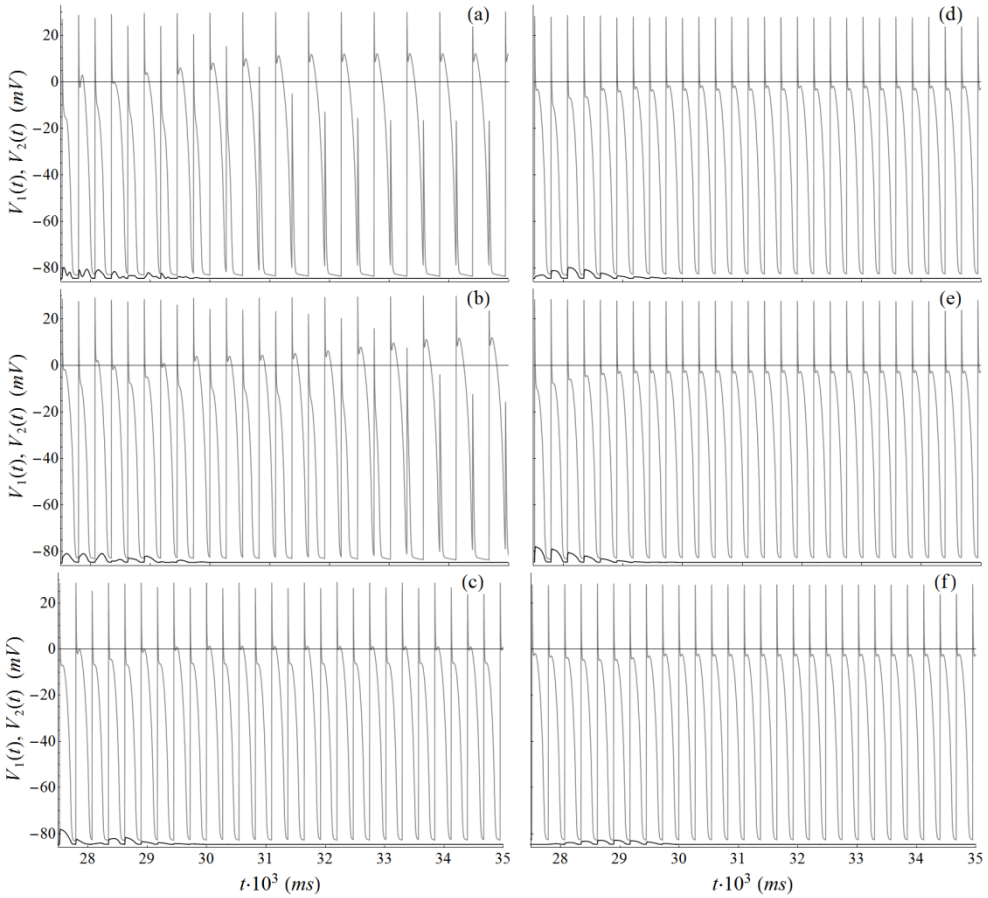

Fig. 10. (a) Action potentials in *Cell* 1 (grey trace) and response of *Cell* 2 (black trace) in the case of progressively decreasing fluctuating coupling just before and immediately after permanent decoupling at $t = 30{,}000$ ms, for stimulus period of 275 ms, $\gamma_0 = 0.05$, and $\delta = 50$ ms; (b) $\delta = 150$ ms; (c) $\delta = 325$ ms; (d) $\delta = 500$ ms; (e) $\delta = 700$ ms; (f) $\delta = 1{,}000$ ms

Specifically, the closer the morphology of the last response to the uncoupled case, the faster the rhythm between stimulus and *Cell* 1 will return to 2:1 (Fig. 10a,b). If, on the other hand, the last response corresponds to two individual APs, then the rhythm is fixed at 1:1 until the end of the numerical solution (Fig. 10c-f). A few exceptions aside, the simulation data also suggest that the transition mainly takes place for the smaller δ values (up to 325 ms). The rhythm between *Cells* 1 and 2 cannot be defined uniquely in all three stimulus period cases (Fig. 8). The aperiodic response of the system in all parameter cases is illustrated in the phase diagrams of Fig. 8 and 9.

4. Discussion

In the present study we developed a mathematical model which describes the degeneration of electrical coupling between two adjacent cells in the context of AVC disease. The model showed that GJ restructuring alone, resulting in attenuation of electrical coupling, is sufficient to initiate arrhythmic episodes, as previously hypothesized (Saffitz 2005). Although experimental data for the restructuring process are currently unavailable, the imposed fluctuation and systematic decrease of electrical coupling between cells in our model may provide insight into disease progression. In particular, the weaker the coupling, the more pronounced the difficulty in AP propagation becomes. This mechanism may pre-exist arrhythmogenesis due to fibrofatty replacement since the latter is gradual and may even not develop if the disease is acute or rapidly progressive (Tsatsopoulou et al. 2006). Furthermore, our simulations suggest aggravation of arrhythmic response between cells upon increase of stimulus frequency, in accordance to experimental data from endurance training of animal models (Kirchhof et al. 2006). The irregular spatio-temporal variation of electrical coupling should allow different responses observed in simulations to emerge. In the three-dimensional electrical syncytium of an AVC affected ventricle, local electrical instability may be amplified and through electrical excitation-mechanical contraction coupling affect the function of the entire heart.

In order to describe the membrane ionic activity and resulting APs, we used the model of Beeler and Reuter (1977). Although we could use more recent and accurate descriptions of membrane ionics (e.g., ten Tusscher et al. 2004), this would render our approach more complex. Since here we focused on the effect of mechanically-induced GJ restructuring on arrhythmogenesis, for simplicity and mathematical transparency, we consider the Beeler-Reuter model sufficient for our purposes.

We deliberately neglected characteristic aspects of GJ biophysical behavior such as the gating mechanisms and the subconductance states (Harris 2001). Although inclusion of gating into our analysis would provide a more realistic description of GJs, it would probably have little qualitative effect on our results. Specifically, the addition of a scheme for closure and reopening of GJs would only intensify the fluctuation of N and subsequently γ, and render the arrhythmic response more pronounced. We did not take into account any subconductance states, the inclusion of which would only lower g and, hence, γ as well. Furthermore, considering $g \approx 100$ pS and a population of 500 always open unit channels resulted in $\gamma = 0.5$. Based on that estimate, we investigated the behavior of the model for values of initial coupling that span from very strong ($\gamma_0 = 0.70$), to very weak ($\gamma_0 = 0.05$). Data from experimental studies suggest, however, that only a small percentage of GJs in a plaque are functional at a given time (Harris 2001). Lowering the initial population of unit channels in our model would readjust γ_0 values accordingly, most probably below γ_u, leading to the elimination of misfire occurrence. The latter may not be pertinent to AVC disease, but to a rather different type of pathology. On the other hand, a downgrade of γ_0 values would, again, intensify attenuation of the coupling and the arrhythmic response, without affecting our conclusions.

We assumed that the cross-sectional area of individual GJ channels in hearts of AVC patients might be reduced. This assumption is based on experimental data from GJ hemichannels, the extracellular parts of which respond to stimuli by reducing the channel diameter (Müller et al. 2002, Thimm et al. 2005).

Our approach in the variation of the GJ population is deliberately exaggerated. In the first step, we considered the heavy fluctuation of electrical coupling between an initial value and zero. Allowing the coupling to reach zero and rebound all the way back to the initial value is probably unrealistic. However, in this way we were able to observe arrhythmic episodes and

describe thoroughly the dependence of the system response on the coupling, for a broad range of parameter values. In the second step, we imposed the gradual decrease of the upper limit of fluctuation with time through the function $w(t)$ and observed a qualitatively similar behavior. Even though the combination of fluctuation and $w(t)$ is arbitrary, this approach is more reasonable and possibly more realistic. Gap junctions are assembled and disassembled even in healthy conditions. In AVC disease, more GJs may be disassembled due to the progressive degradation of intercellular mechanical coupling, and less may be assembled due to the diminishing of Connexin43 in ICDs. This process is probably not continuous but rather episodic, which accounts for the fluctuation as well; otherwise the failure in AP propagation would be permanent after its first occurrence. Finally, δ values employed for the construction of the interpolation functions are also arbitrary and are chosen in regard of the duration of the Beeler-Reuter AP.

In summary, our model shows that in AVCs the restructuring of GJ channels severely impairs the electrical coupling of ventricular cells and thus provokes arrhythmogenesis. Such heart muscle disorders are the result of various pathogenic mechanisms that do not preclude each other. Hence, GJ restructuring may pre-exist the electrical instability due to replacement of dying myocytes by fibrofatty tissue as a main cause of arrhythmia. While the model successfully predicts the deficiency in AP generation and propagation, consistent with the emergence of lethal ventricular arrhythmias in AVC patients, experimental data regarding the variation of GJ population and the deformation of individual channels are needed to further support the model.

Acknowledgements This work is supported by the National Heart, Blood and Lung Institute grant HL 096005.

Appendices

A. The beeler-reuter model

The membrane ionics for each cell follow the Beeler-Reuter model for mammalian ventricular myocardial cells. According to Beeler and Reuter (1977), the ionic channel current density (I^{ion}) is generated by: an inward Na^+ current (I_{Na}); a time-independent (I_K) and a time-activated outward (I_x) K^+ current; and a slow inward Ca^{2+} current (I_S); i.e.,

$$I^{ion} = I_{Na} + I_K + I_x + I_S. \tag{A1}$$

The explicit equations of the ionic currents, in ($\mu A/cm^2$), are given as follows (Keener and Sneyd 2009b).

$$I_{Na} = (G_{Na}\, m^3\, h\, j + 0.003)\,(V - 50), \tag{A2}$$

$$I_K = 1.4\frac{e^{0.04(V+85)} - 1}{e^{0.08(V+53)} + e^{0.04(V+53)}} + 0.07\frac{V + 23}{1 - e^{-0.04(V+23)}}, \tag{A3}$$

$$I_x = 0.8\, x\frac{e^{0.04(V+77)} - 1}{e^{0.04(V+35)}}, \tag{A4}$$

$$I_S = G_S \; f \; d \; (V + 82.3 + 13.0287 \ln[Ca]_i), \tag{A5}$$

where V is given in (mV), and time is measured in (ms); G_{NA} = 4 mS/cm^2, G_S = 0.09 mS/cm^2; the parameters m, h, j, x, f, and d, are time-dependent gating (activation-inactivation) variables, and the intracellular Ca^{2+} concentration (c) is tracked by the equation

$$\frac{dc}{dt} = 0.07\left(1 - c\right) - I_S, \tag{A6}$$

with $c = 10^7$ $[Ca]_i$. The time dependence of the gating variables is expressed through the general equations:

$$\frac{dz}{dt} = \alpha_z (1 - z) - \beta_z \; z, \tag{A7}$$

where $z = m, h, j, x, f, d$. The α_z and β_z are defined by algebraic expressions of the form

$$\alpha_z, \beta_z = \frac{C_1 \, \mathrm{e}^{\frac{V - V_0}{C_2}} + C_3 (V - V_0)}{1 + C_4 \, \mathrm{e}^{\frac{V - V_0}{C_5}}}. \tag{A8}$$

The values for coefficients C_1-C_5 and V_0 can be found in Beeler and Reuter (1977), or Keener and Sneyd (2009b).

B. Interpolation function $F_\delta(t)$

We construct a set of k points (t_k, n_k), where k is determined by dividing the solution range by the length of the time interval (δ) between two successive points. Here, t_k are time instances distributed uniformly across the entire solution range with $t_1 = 0$; n_k are randomly generated numbers such that $n_k \in [0,1]$ with $n_1 = 1$. We then construct the approximate function $F_\delta(t)$ that interpolates the set of points such that $F_\delta(t) \in [0,1]$ and $F_\delta(0) = 1$. The rate of variation of $F_\delta(t)$ (and hence $\gamma(t)$ as well) depends on the value of δ; the smaller the δ the faster the variations of $\gamma(t)$. Since there are no available data on the time scale of dynamics of GJ restructuring during disease, we consider arbitrary values of δ = 50, 150, 325, 500, 700, and 1,000 ms, which in increasing order correspond from relatively faster to slower variations of $\gamma(t)$ (Fig. 3).

Извод

Математички модел аритмогенезе код вентрикуларне кардиомиопатије услед реструктурирања пропусне везе

A. P. Pirentis[1], D. Stamenović[2]*

Department of Biomedical Engineering, Boston University, 44 Cummington St., Boston, MA 02215, USA.
[1]thanospp@bu.edu
[2]dimitrij@bu.edu
**Corresponding author*

Резиме

Генетски дефекти на местима контакта између ћелија су повезани са аритмогеном вентрикуларном кардиомиопатиом (eng. arrhythmogenic ventricular cardiomyopathies - AVCs) и познато је да ометају спрезање ћелија. Клиничка запажања код пацијената са AVC-ом су открила замену здравог срчаног ткива влакнасто-масним ткивом, што ствара анатомску подлогу за аритмију, прогресивно срчано оштећење и изненадну смрт. Са друге стране, одсуство влакнасто-масног ткива у срцу код младих пацијената и у неким варијантама AVC-а сугерише да се озбиљне аритмије могу јавити услед реструктурирања пропусних веза (gap junctions - GJs) у окружењу деградираног механичког спрезања између кардиомиоцита. У овом раду смо развили математички модел у циљу истраживања ефекта GJ реструктурирања на аритмогенезу код AVC-а. Разматран је пар вентрикуларних ћелија и симулиран је ефекат GJ реструктурирања при случајној флуктуацији проводности електричне спреге. Појава приметних епизода аритмије је брзо забележена. Даљим смањењем опсега флуктуације током времена, пропагација је изостајала и генерисање акционог потенцијала је престало чак и пре престанка стимулације. Резултати симулације модела одговарају клиничким запажањима, што сугерише постојање алтернативног механизма за генерисање смртоносне вентрикуларне аритмије код AVC-а.

Кључне речи: спрегнуте ћелије, акциони потенцијал, пропусна веза, аритмогенска вентрикуларна кардиомиопатија, нумеричка симулација

References

Asimaki A, Syrris P, Wichter T, Matthias P, Saffitz JE, McKenna WJ (2007). A novel dominant mutation in plakoglobin causes arrhythmogenic right ventricular cardiomyopathy, *American* Journal *of Human Genetics*, 81(5), 964-973.

Beeler GW, Reuter H (1977). Reconstruction of the action potential of ventricular myocardial fibres, *Journal of Physiology*, 268(1), 177-210.

de Groot JR, Veenstra T, Verkerk AO, Wilders R, Smits JPP, Wilms-Schopman FJG, Wiegerinck RF, Bourier J, Belterman CNW, Coronel R, Verheijck EE (2003). Conduction

slowing by the gap junctional uncoupler carbenoxolone, *Cardiovascular Research*, 60(2), 288-297.

Harris AL (2001). Emerging issues of connexin channels: biophysics fills the gap, *Quarterly Reviews of Biophysics*, 34(3), 325-472.

Huang H, Asimaki A, Lo D, McKenna WJ, Saffitz J (2008). Disparate effects of different mutations in plakoglobin on cell mechanical behavior, *Cell Motility and the Cytoskeleton*, 65(12), 964–978.

Huelsing DJ, Pollard AE, Spitzer KW (2001). Transient outward current modulates discontinuous conduction in rabbit ventricular cell pairs, *Cardiovascular Research*, 49(4), 779-789.

Jensen JH, Christiansen PL, Scott AC, Skovgaard O (1984). Chaos in the Beeler-Reuter system for the action potential of ventricular myocardial fibres, *Physica D*, 13(1-2), 269-277.

Joyner RW, Kumar R, Wilders R, Jongsma HJ, Verheijck EE, Golod DA, van Ginneken ACG, Wagner MB, Goolsby WN (1996). Modulating L-type calcium current affects discontinuous cardiac action potential conduction, *Biophysical Journal*, 71(1), 237-245.

Joyner RW, Sugiura H, Tan RC (1991). Unidirectional block between isolated rabbit ventricular cells coupled by a variable resistance, *Biophysical Journal*, 60(5), 1038-1045.

Kaplan SR, Gard JJ, Carvajal-Huerta L, Ruiz-Cabezas JC, Thiene G, Saffitz JE (2004b). Structural and molecular pathology of the heart in Carvajal syndrome, *Cardiovascular Pathology*, 13(1), 26– 32.

Kaplan SR, Gard JJ, Protonotarios N, Tsatsopoulou A, Spiliopoulou C, Anastasakis A, Squarcioni CP, McKenna WJ, Thiene G, Basso C, Brousse N, Fontaine G, Saffitz JE (2004a). Remodeling of myocyte gap junctions in arrhythmogenic right ventricular cardiomyopathy due to a deletion in plakoglobin (Naxos disease), *Heart Rhythm*, 1(1), 3–11.

Keener J, Sneyd J (2009a). *Mathematical Physiology I: Cellular Physiology*, second edition, Springer, New York, NY, USA.

Keener J, Sneyd J (2009b). *Mathematical Physiology II: Systems Physiology*, second edition, Springer, New York, NY, USA.

Keener JP (1990). The effects of gap junctions on propagation in myocardium: a modified cable theory, *Annals of the New York Academy of Sciences*, 591(1), 257-277.

Kirchhof P, Fabritz L, Zwiener M, Witt H, Schäfers M, Zellerhoff S, Paul M, Athai T, Hiller K, Baba HA, Breithardt G, Ruiz P, Wichter T, Levkau B (2006). Age- and training-dependent development of arrhythmogenic right ventricular cardiomyopathy in heterozygous plakoglobin-deficient mice, *Circulation*, 114(17), 1799-1806.

McKoy G, Protonotarios N, Crosby A, Tsatsopoulou A, Anastasakis A, Coonar A, Norman M, Baboonian C, Jeffery S, McKenna WJ (2000). Identification of a deletion in plakoglobin in arrhythmogenic right ventricular cardiomyopathy with palmoplantar keratoderma and woolly hair (Naxos disease), *Lancet*, 355(9221), 2119–2124.

Morley GE, Anumonwo JM, Delmar M (1992). Effects of 2,4-dinitrophenol or low $[ATP]_i$ on cell excitability and action potential propagation in guinea pig ventricular myocytes, *Circulation Research*, 71(4), 821-830.

Müller DJ, Hand GM, Engel A, Sosinsky GE (2002). Conformational changes in surface structures of isolated connexin 26 gap junctions, *EMBO Journal*, 21(14), 3598-3607.

Peercy BE, Keener JP (2005). Coupled cell model of border zone arrhythmias, *SIAM Journal on Applied Dynamical Systems*, 4(3), 679-710.

Protonotarios N, Tsatsopoulou A (2004). Naxos disease and Carvajal syndrome: Cardiocutaneous disorders that highlight the pathogenesis and broaden the spectrum of arrhythmogenic right ventricular cardiomyopathy, *Cardiovascular Pathology*, 13(4), 185–194.

Ruiz P, Brinkmann V, Ledermann B, Behrend M, Grund C, Thalhammer C, Vogel F, Birchmeier C, Günthert U, Franke WW, Birchmeier W (1996). Targeted mutation of plakoglobin in mice reveals essential functions of desmosomes in the embryonic heart, *Journal of Cell Biology*, 135(1), 215-225.

Saffitz JE (2005). Dependence of electrical coupling on mechanical coupling in cardiac myocytes: insights gained from cardiomyopathies caused by defects in cell-cell connections, *Annals of the New York Academy of Sciences*, 1047(1), 336-344.

Schnittler H-J, Püschel B, Drenckhahn D (1997). Role of cadherins and plakoglobin in interendothelial adhesion under resting conditions and shear stress, *American Journal of Physiology - Heart and Circulatory Physiology*, 273(5), H2396-H2405.

Sugiura H, Joyner RW (1992). Action potential conduction between guinea pig ventricular cells can be modulated by calcium current, *American Journal of Physiology - Heart and Circulatory Physiology*, 263(5), H1591-H1604.

Tan RC, Joyner RW (1990). Electrotonic influences on action potentials from isolated ventricular cells, *Circulation Research*, 67(5), 1071-1081.

Tan RC, Osaka T, Joyner RW (1991). Experimental model of effects on normal tissue of injury current from ischemic region, *Circulation Research*, 69(4), 965-974.

ten Tusscher KHWJ, Noble D, Noble PJ, Panfilov AV (2004). A model for human ventricular tissue, *American Journal of Physiology - Heart and Circulatory Physiology*, 286(4), H1573-H1589.

Thimm J, Mechler A, Lin H, Rhee S, Lal R (2005). Calcium dependent open/closed conformations and interfacial energy maps of reconstituted hemichannels, *Journal of Biological Chemistry*, 280(11), 10646-10654.

Tsatsopoulou AA, Protonotarios NI, McKenna WJ (2006). Arrhythmogenic right ventricular dysplasia, a cell adhesion cardiomyopathy: insights into disease pathogenesis from preliminary genotype-phenotype assessment, *Heart*, 92(12), 1720-1723.

Wang Y-G, Wagner MB, Kumar R, Goolsby WN, Joyner RW (2000). Fast pacing facilitates action potential propagation between rabbit atrial cells," *American Journal of Physiology - Heart and Circulatory Physiology*, 279(5), H2095-H2103.

Weingart R, Maurer P (1988). Action potential transfer in cell pairs isolated from adult rat and guinea pig ventricles, *Circulation Research*, 63(1), 72-80.

Wilders R, Kumar R, Joyner RW, Jongsma HJ, Verheijck EE, Golod DA, van Ginneken ACG, Goolsby WN (1996). Action potential conduction between a ventricular cell model and an isolated ventricular cell, *Biophysical Journal*, 70(1), 281-295.

Yin T, Getsios S, Caldelari R, Godsel LM, Kowalczyk AP, Müller EJ, Green KJ (2005). Mechanisms of plakoglobin-dependent adhesion: desmosome-specific functions in assembly and regulation by epidermal growth factor receptor, *Journal of Biological Chemistry*, 280(48), 40355-40363.